



## ORIGINAL ARTICLE

# Preparation of the Mn-Fe-Ce/ $\gamma$ -Al<sub>2</sub>O<sub>3</sub> ternary catalyst and its catalytic performance in ozone treatment of dairy farming wastewater

Jiayao Li, Weifeng Song<sup>\*</sup>, Zefeng Yu, Qiuhua Li

School of Environmental Science and Engineering, Guangdong University of Technology, Guangzhou 510006, PR China

Received 4 December 2019; accepted 5 January 2020

Available online 13 January 2020

## KEYWORDS

Mn-Fe-Ce/ $\gamma$ -Al<sub>2</sub>O<sub>3</sub>;  
Refractory organics;  
Dairy farming wastewater;  
Catalytic ozonation;  
HO<sup>•</sup>

**Abstract** The quality of dairy farming wastewater in different regions is particular and different. In Southern China, the Chemical Oxygen Demand (COD<sub>Cr</sub>) and colourity of effluent from conventional dairy farming wastewater treatment processes are similar. Catalytic ozonation is a very promising technical method. In this paper, the Mn-Fe-Ce/ $\gamma$ -Al<sub>2</sub>O<sub>3</sub> catalyst was prepared via the optimized preparation method of impregnation roasting using  $\gamma$ -Al<sub>2</sub>O<sub>3</sub> as the carrier, and this catalyst was used in the ozonation of actual dairy farming wastewater from treatment facilities. The performance of the Mn-Fe-Ce/ $\gamma$ -Al<sub>2</sub>O<sub>3</sub> catalyst on dairy farming wastewater was investigated using a simulated dynamic test. The effects of the reaction time, pH and catalyst dosage on COD<sub>Cr</sub> and the colourity removal ratio were investigated. The results show that the optimum treatment conditions were a reaction time of 20 min, pH 9, and catalyst dosage of 15 g/L. The COD<sub>Cr</sub> removal ratio reached 48.9% and the colourity was 95% under the optimum conditions. BOD<sub>5</sub>/COD<sub>Cr</sub> increased from 0.21 to 0.54 after catalytic ozonation, indicating that the biodegradability of wastewater was significantly improved. This research provides a new method and theoretical guidance for dairy farming wastewater treatment.

© 2020 The Author(s). Published by Elsevier B.V. on behalf of King Saud University. This is an open access article under the CC BY-NC-ND license (<http://creativecommons.org/licenses/by-nc-nd/4.0/>).

## 1. Introduction

Livestock and poultry farming have been developed rapidly as an important part of agricultural production. Large-scale farming has become the major method of livestock and poultry breeding in recent decades in southern China. In recent years, increasing focus has been given to the treatment of livestock and poultry wastewater (Kuang et al., 2019; Santos et al., 2019). The traditional methods for treating livestock and poultry wastewater mainly include returning to field, ecological restoration and biochemical treatment technologies (Khin and Annachhatre, 2004; Li and Zhang, 2002), but the removal of polycyclic organic substances from wastewater is not effective due to its complex molecular structure, stable chemical properties, and the inability of

<sup>\*</sup> Corresponding author.

E-mail address: [weifengsong@gdut.edu.cn](mailto:weifengsong@gdut.edu.cn) (W. Song).

Peer review under responsibility of King Saud University.



Production and hosting by Elsevier

traditional methods. The effluent COD<sub>Cr</sub> and colourity remain high. Dairy farming wastewater contains high concentrations of organics, ammonia nitrogen and suspended solids and a considerable number of pathogens and toxic substances of specific structure (Juteau et al., 2004; Yang et al., 2003). After aerobic treatment, which is the main source of pollution of surface water and groundwater, the colourity also sharply increases (Ferreira et al., 2003). Refractory organics in dairy farming wastewater, which is the key factor of dairy farming wastewater treatment in southern China, has not been reported to date.

Oxidation by ozone has been widely used to improve the biodegradability of organic wastewater and the decolorization of chromogenic wastewater given its high efficiency, cost, easy operation and obvious decolorization effect (Huang et al., 2019; Wang et al., 2019). The sole ozonation process has the disadvantages of low ozone utilization efficiency, poor pollutant removal efficiency, and high cost (Faria et al., 2008). Under heterogeneous catalysis conditions, studies have shown it can promote the conversion of ozone to hydroxyl radicals (HO<sup>•</sup>) and improve ozone utilization and organic mineralization efficiency (Ikhtlaq et al., 2013; Nie et al., 2014; Nie et al., 2015). In addition, the catalyst exists in solid form, and the metal elements are not dissolved in weak acid to weak alkali conditions (Feng et al., 2018; Wu et al., 2011). Therefore, heterogeneous catalytic ozonation technology has the advantages of simple process flow, reusability, easy separation and high catalytic efficiency (Armenta et al., 2018; Maleki et al., 2016a; Rodríguez et al., 2012; Ziyilan-Yavaş and Ince, 2018). The recovery and reusability of heterogeneous catalysts is an important factor in green chemistry (Maleki, 2018; Maleki et al., 2018; Maleki et al., 2016b; Najafian et al., 2015). Heterogeneous catalytic ozonation has been employed in many studies, which have been confirmed that treatment effect is significantly better than that of sole ozonation (Aihua et al., 2010; Ncanana and Rajasekhar Pullabhotla, 2019; Sun et al., 2019). However, the preparation of Mn-Fe-Ce/ $\gamma$ -Al<sub>2</sub>O<sub>3</sub> catalysts and its catalytic performance in ozonation remain unknown, especially in the treatment of dairy farming wastewater. The catalytic performance of Mn-Fe-Ce/ $\gamma$ -Al<sub>2</sub>O<sub>3</sub> ternary catalyst and degradation mechanisms of refractory organics in the system are worthy of further investigation.

In this work, supported Mn-Fe-Ce/ $\gamma$ -Al<sub>2</sub>O<sub>3</sub> catalysts were prepared by an incipient wetness impregnation procedure followed by drying and calcination in muffle furnace. The preparation conditions and process conditions were optimized. The structure and physicochemical properties of the catalysts were characterized using SEM, XRF, XRD and BET methods. Microbubble ozone constitutes a heterogeneous catalytic ozonation system in the experiment.

## 2. Materials and methods

### 2.1. Preparation of catalysts

The  $\gamma$ -Al<sub>2</sub>O<sub>3</sub> pellets were washed with deionized water, placed in an oven, and dried at 65 °C. The ternary catalyst was prepared using the immersion roasting method, and the 1% aqueous solution of manganese nitrate, 1% aqueous solution of ferric nitrate and 1.5% aqueous solution of cerous nitrate were dissolved in distilled water and thoroughly stirred. The volume was brought to 100 mL. For precursor impregnating solution, 20 g  $\gamma$ -Al<sub>2</sub>O<sub>3</sub> pellets were immersed in the precursor impregnation liquid and subjected to shaking impregnation and static impregnation. Shaking was performed for 12 h. The shaking conditions were as follows: shaking temperature was 30 °C, shaking speed was 180 rpm; and static immersion 12 h. The static conditions involved incubation of the sample at 30 °C. Thus, the metal was supported on the surface of the  $\gamma$ -Al<sub>2</sub>O<sub>3</sub> pellet. The catalyst was removed from the mother

solution and placed in an oven at 65 °C for 12 h. The dried catalyst was placed in a crucible and heated up to 600 °C. The sample was roasted in a muffle furnace for 4 h. After calcination, a ternary supported Mn-Fe-Ce/ $\gamma$ -Al<sub>2</sub>O<sub>3</sub> catalyst was obtained.

### 2.2. Wastewater and reagents

The wastewater used in the experiment is actual wastewater obtained from the first-stage aerobic tank of a dairy farming based in Guangzhou. The average COD<sub>Cr</sub> is 460 mg/L, and the biodegradability is low. The COD<sub>Cr</sub> of the secondary biochemical pool is minimally reduced, and the organics are difficult to obtain.

The  $\gamma$ -Al<sub>2</sub>O<sub>3</sub> carrier was purchased from Jiangsu Sanji Industrial Co., Ltd, Taizhou, Jiangsu, China. Manganese nitrate solution, ferric nitrate nonahydrate, and cerous nitrate hexahydrate were purchased from Shanghai Aladdin Biochemical Technology Co., Ltd, Shanghai, China. TBA was purchased from Tianjin Damao Chemical Reagent Co., Ltd, Tianjin, China. The ozone generator was purchased from Guangzhou Chuanghuan Ozone Electric Equipment Co., Ltd, Guangzhou, Guangdong, China (model CH-ZTW5G).

### 2.3. Characterization of catalysts

The microscopic morphology of the catalyst was observed using a field emission scanning electron microscope (SEM, SU8220, Hitachi, Japan). The content of the element in the catalyst was measured using an energy dispersive X-ray fluorescence spectrometer (XRF, EDX-7000, Shimadzu Corporation, Japan). The specific surface area of the catalyst was measured using a fully automated rapid surface to porosity analyzer (BET, model ASAP2460, Micromeritics, USA). The crystal structure of the catalyst was analyzed using an X-ray diffractometer (XRD, model D8 ADVANCE, Bruker, Germany).

### 2.4. Experimental methods

The equipment used in the experiment is shown in Fig. 1. The ozone reactor is composed of two homemade plexiglass reactors. The left reactor has a height of 300 mm, a diameter of 120 mm, and an effective volume of 4 L. At a height of 80 mm, a stainless steel porous dispersion network with a diameter of 2 mm is installed, and the gas distribution device is a micro-scale aeration head at the bottom of the reactor. The right reactor has a height of 200 mm and a diameter of 100 mm. A submersible pump (model HJ-611) is installed inside.

All experiments were performed at room temperature in a semi-continuous manner. Approximately 3.6 L of wastewater was poured into the right reactor, and the submersible pump was turned on to allow the wastewater from the right container to enter the left reactor until the desired water level was attained. At the location of the nozzle, the wastewater flows into the right container again, and the wastewater forms a circulating flow state, which is conducive to the mixing of ozone and wastewater. The effects of different reaction conditions on the catalytic effect were studied by controlling different reaction times, pH and catalyst dosages. During the reaction, the

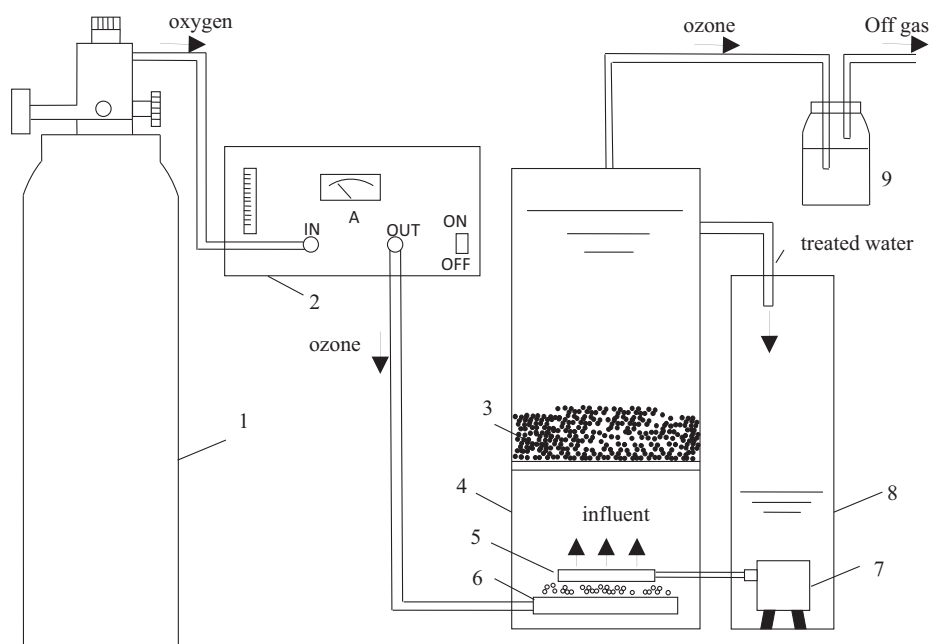


**Fig. 1** Schematic diagram of microbubble ozone catalytic oxidation (1:99.99% pure oxygen, 2: Ozone generator, 3: Catalyst, 4: Reactor, 5: Water distribution device, 6: Micron aeration head, 7: Submersible pump, 8: Reflux container, 9: KI).

pH will change slightly during the experiment for the reason that ozone will consume the hydroxide. Therefore, we use the 5% NaOH and 5 mol/L  $H_2SO_4$  to control the pH value during the experiment of different pH conditions. Samples were obtained at 5, 10, 15 and 20 min to measure  $COD_{Cr}$  and colourity.

### 3. Results and discussion

#### 3.1. Characterization of catalysts

Fig. 2(a)–(d) present the SEM photographs of the Mn-Fe-Ce/ $\gamma-Al_2O_3$  catalyst and  $\gamma-Al_2O_3$  at 5  $\mu m$  and 1  $\mu m$ , respectively. The surface of the two materials exhibits different morphological features.

Fig. 2(a)–(b) demonstrate that the surface of the Mn-Fe-Ce/ $\gamma-Al_2O_3$  catalyst exhibits elliptical fine particles that are baked by impregnation. The resulting active component is obviously attached to the surface of the carrier. This indicated that the catalyst have undergone a physicochemical reaction during the preparation procedures to form a metal oxide (Feng et al., 2000). The selected area in Fig. 2(b) is scanned by SEM-EDX spectrum, and the element content is shown in Fig. 2(e). In Fig. 2(c)–(d), the surface of the  $\gamma-Al_2O_3$  carrier is obviously smooth, and some irregular small particles are sparsely distributed. In summary, the results of Fig. 2(a)–(d) demonstrated successful active component loading.

The elemental composition of the Mn-Fe-Ce/ $\gamma-Al_2O_3$  catalyst and  $\gamma-Al_2O_3$  was analyzed by XRF spectroscopy. The results are shown in Fig. 3.

In addition to the main element Al in the Mn-Fe-Ce/ $\gamma-Al_2O_3$  catalyst, the percentage composition of Fe, Mn, and Ce were detected to be 17.6%, 11.7%, and 10.2%. In  $\gamma-Al_2O_3$ , only more than 90% of Al and other elements were detected, while Fe, Mn, and Ce were not found. The results

indicating that Fe, Mn, and Ce can be effectively supported on the surface of  $\gamma-Al_2O_3$ . These results are consistent with SEM results.

The XRD patterns of Mn-Fe-Ce/ $\gamma-Al_2O_3$  catalyst and  $\gamma-Al_2O_3$  are shown in Fig. 4. In Fig. 4(b), the diffraction peaks at  $2\theta = 37.441^\circ, 39.672^\circ, 42.823^\circ, 45.788^\circ, 60.457^\circ, 67.306^\circ,$  and  $85.005^\circ$  coincide with the characteristic peaks of  $Al_2O_3$  in the JCPDS standard card and exhibit the same intensity. In Fig. 4(a), it can be clearly seen that the diffraction angle is  $28^\circ$ – $30^\circ$ , and some diffraction peaks appear at  $32^\circ$ . The characteristic peak of  $Al_2O_3$  is also observed. As seen from the standard card, the diffraction angle is  $28.68^\circ$ . The characteristic peak belongs to amorphous  $MnO_2$ , the characteristic peak of  $31.0^\circ$  belongs to  $Fe_2O_3$ , and the characteristic peak of  $28.7^\circ$  belongs to  $Ce_2O_3$ . However, the intensity of the detected diffraction peaks is weak, which may be related to the loading amount and the crystallization effect.

As shown in Table 1, the BET test was performed on the Mn-Fe-Ce/ $\gamma-Al_2O_3$  catalyst and  $\gamma-Al_2O_3$ . Compared with  $\gamma-Al_2O_3$ , the  $\gamma-Al_2O_3$  catalyst loaded with Mn, Fe and Ce exhibits a reduction in specific surface area and total pore volume because some of the pores and gaps on the carrier were occupied after the loading of the active component (He et al., 2018). This finding is also confirmed by SEM analysis.

#### 3.2. Effects of reaction time on catalytic ozonation using Mn-Fe-Ce/ $\gamma-Al_2O_3$

When the gas flow ratio and ozone concentration of the ozone generator are kept constant, different reaction times represent different amounts of ozone, and the effect of heterogeneously catalytic ozonation on dairy farming wastewater is also different. Mn-Fe-Ce/ $\gamma-Al_2O_3$  was used to catalyze the ozonation of dairy farming wastewater.  $COD_{Cr}$  and colourity were determined at the reaction time points of 0, 5, 10, 15, 20, 25 and

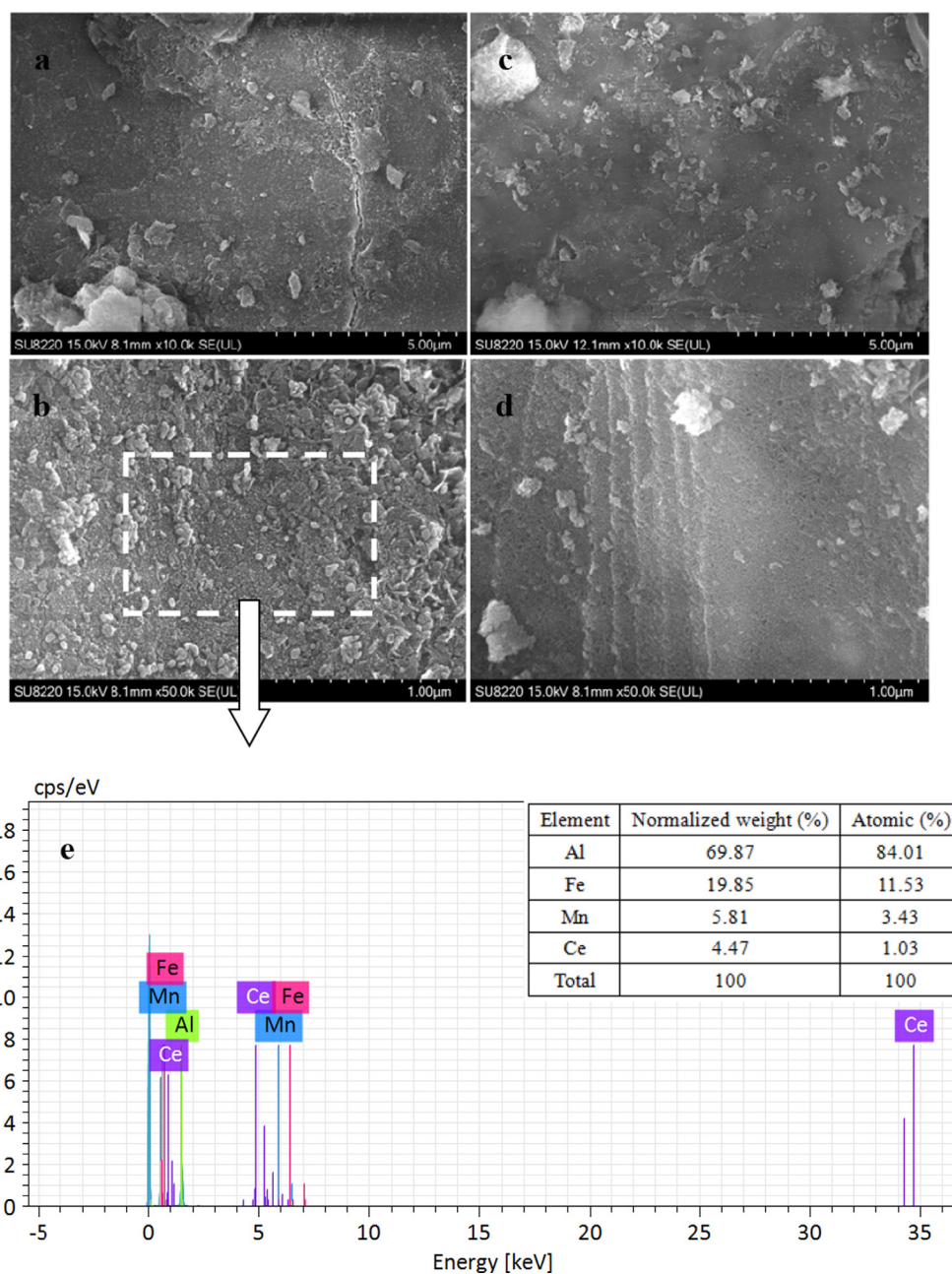


**Fig. 2** SEM images of Mn-Fe-Ce/ $\gamma$ -Al<sub>2</sub>O<sub>3</sub> catalyst (a)–(b);  $\gamma$ -Al<sub>2</sub>O<sub>3</sub> (c)–(d); SEM-EDX spectrum (e) of the area indicated in (b).

30 min, and the COD<sub>Cr</sub> removal ratio and colourity removal ratio were calculated. These values can be used to investigate the optimum reaction time of Mn-Fe-Ce/ $\gamma$ -Al<sub>2</sub>O<sub>3</sub> for ozonation of dairy farming wastewater.

The duration of the reaction determines the cost input in the process and the hydraulic retention time of the treatment process. Therefore, it is concluded that the optimal reaction time for catalytic ozonation of dairy farming wastewater is of great significance in engineering applications of heterogeneous catalytic ozonation technology. During the experiment, the inlet flow ratio of the ozone generator was adjusted to 0.6 L/min, and the ozone concentration was 75 mg/L. The whole reaction process remained unchanged to ensure the optimal reaction time under the condition of certain ozone concentrations. The experimental results are shown in Fig. 5.

The COD<sub>Cr</sub> removal ratio and colourity removal ratio increased with the reaction time. When the reaction time was 30 min, the COD<sub>Cr</sub> value of dairy farming wastewater decreased to 229 mg/L, the COD<sub>Cr</sub> removal ratio reached 50.1%, and the colourity removal ratio reached 95%. At 20 min and 25 min, the COD<sub>Cr</sub> removal ratio was 48.9% and 49.4%, and the colourity removal ratio was 95%. During the reaction period of 20 to 30 min, the COD<sub>Cr</sub> removal ratio only increased by 1.2%, and the colourity removal ratio did not change. Thus, in the process of heterogeneously catalytic ozonation treatment of dairy farming wastewater, a longer oxidation reaction time increases the ozone dosage and enhances the ozonation effect. However, as time increases, COD<sub>Cr</sub> decreases less and less per unit time because the ozone utilization efficiency decreases. This finding is attributed to the fact

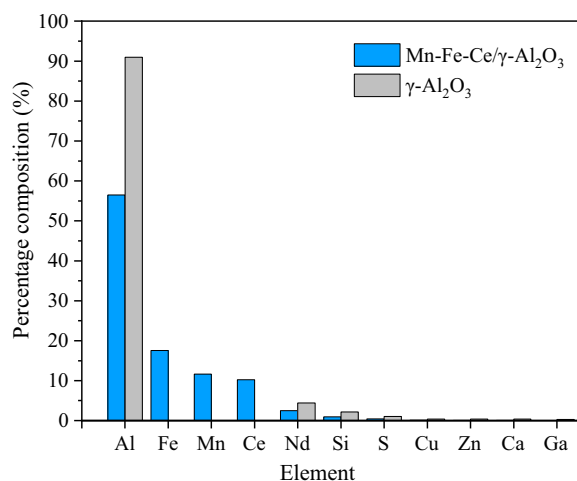


Fig. 3 XRF analysis of Mn-Fe-Ce/γ-Al<sub>2</sub>O<sub>3</sub> catalyst and γ-Al<sub>2</sub>O<sub>3</sub>.

that the oxidant is in close contact with the pollutants, leading some of the pollutants are mineralized to form CO<sub>2</sub>. Meanwhile, carbonate and bicarbonate are formed in the water. These molecules are effective HO<sup>•</sup> inhibitors that reduce the amount of HO<sup>•</sup> in the Mn-Fe-Ce/γ-Al<sub>2</sub>O<sub>3</sub> + O<sub>3</sub> system. However, due to the limited concentration, it is impossible to fully capture all the HO<sup>•</sup> produced by the system. In addition, during the heterogeneously catalytic ozonation process, the macromolecular organic matter is oxidized to a ring-opened state and is cleaved into aliphatic small molecule organic compounds, such as carboxylic acid and alcohol. In the initial stage of the reaction, the catalyst has more active surface sites, and the ozone is decomposed into HO<sup>•</sup>. The reduction of COD<sub>Cr</sub> is also relatively large. As the reaction time increases, the surface active sites of the catalyst are reduced because they were attached by the small molecules that are not mineralized in the early stage. These features cause the slower ozone decomposition ratio, and the ratio of the increase in the COD<sub>Cr</sub> removal ratio and the colourity removal ratio decreased. Based on the cost and removal ratio, the optimum reaction time of Mn-Fe-Ce/γ-Al<sub>2</sub>O<sub>3</sub> catalytic ozonation of dairy farming wastewater was 20 min.

### 3.3. Effects of pH on catalytic ozonation using Mn-Fe-Ce/γ-Al<sub>2</sub>O<sub>3</sub>

The difference in pH in the system directly altered the total concentration of HO<sup>•</sup>, which affects the catalytic activity of heterogeneously catalytic ozonation on dairy farming wastewater. The effect of catalytic ozonation at pH 3, 5, 7, 9, and 11 was examined under the reaction time of 20 min. Fig. 6 demonstrates that the COD<sub>Cr</sub> removal ratio of dairy farming wastewater at pH 3, 5, 7, 9, and 11 after reaction for 20 min were 14.9%, 22.5%, 25.3%, 48.9%, and 18.1%, respectively. The highest value was noted at pH 9. The colourity removal ratio was also highest at pH 9.

There are two main methods in which ozone reacts with pollutants in water, namely direct reaction of ozone and indirect reaction of ozone decomposition to produce HO<sup>•</sup>. The experimental results at pH 3 and 5 demonstrated that under acidic conditions, ozone is relatively stable, and most ozone exists in water in a molecular form. Therefore, the reaction is mainly a direct reaction. The color-developing organics in water were not destroyed, so the COD<sub>Cr</sub> removal ratio and colourity removal ratio exhibited low levels. Under alkaline conditions, ozone is unstable and easily decomposes to form HO<sup>•</sup>, which mainly occurs via an indirect reaction. The indirect reaction of ozone belongs to the radical reaction, and the decomposition produces free radicals at a rapid ratio, which can initiate a chain reaction and allow many organic substances to be mineralized. The reaction equation is reported below (Salla et al., 2018; Sehested et al., 1984).



It can be seen from the above formula that ozone reacts with OH<sup>-</sup> in aqueous solution to form HO<sub>2</sub><sup>-</sup> ions, and HO<sub>2</sub><sup>-</sup> further induces a chain reaction of ozone decomposition. This process produces more HO<sup>•</sup>, which is beneficial to COD<sub>Cr</sub> removal. This finding can also be confirmed from the above experimental results obtained at a pH of 9. However, at a pH of 11, the excessive OH<sup>-</sup> in the system causes the HO<sup>•</sup> concentration in the Mn-Fe-Ce/γ-Al<sub>2</sub>O<sub>3</sub> + O<sub>3</sub> system to increase

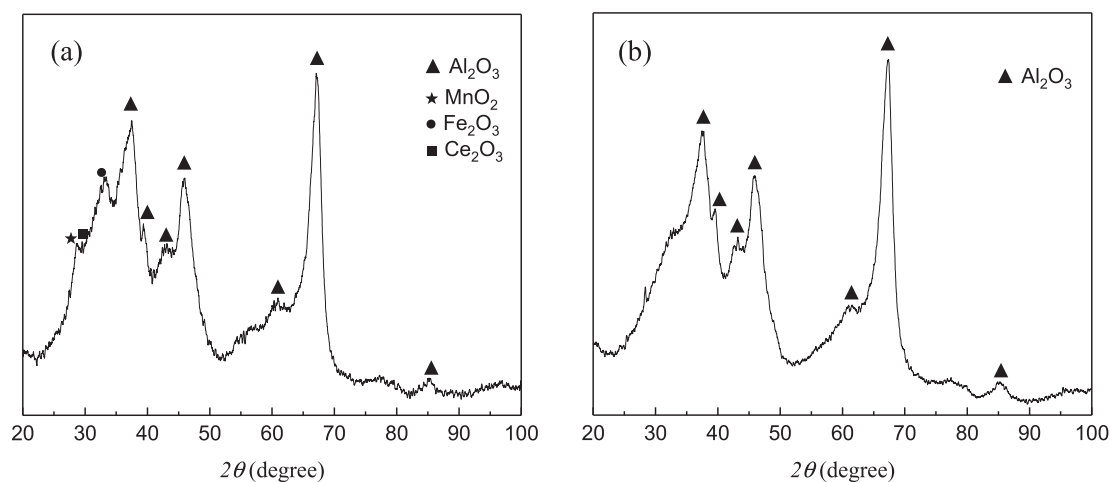
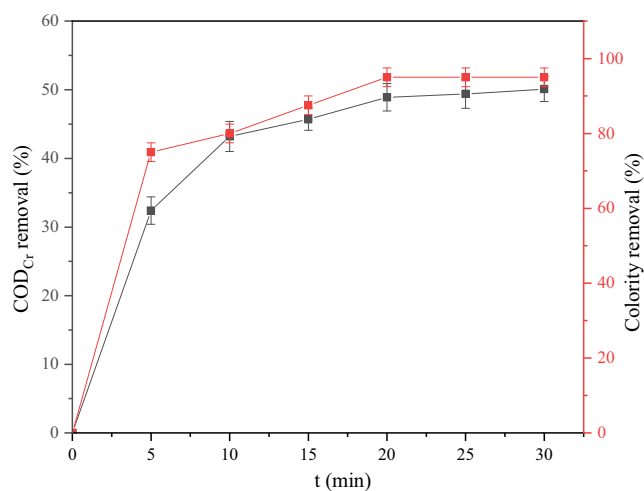


Fig. 4 XRD patterns of Mn-Fe-Ce/γ-Al<sub>2</sub>O<sub>3</sub> (a) and γ-Al<sub>2</sub>O<sub>3</sub> (b).

**Table 1** Analysis of specific surface area and total pore volume of the catalyst.

Catalysts	BET Surface Area (m <sup>2</sup> /g)	BJH Surface Area (m <sup>2</sup> /g)	Total pore volume (cm <sup>3</sup> /g)	Pore Size (nm)
Mn-Fe-Ce/ $\gamma$ -Al <sub>2</sub> O <sub>3</sub>	159.97	87.49	0.046	1.052
$\gamma$ -Al <sub>2</sub> O <sub>3</sub>	200.21	112.86	0.060	1.056

**Fig. 5** COD<sub>Cr</sub> removal ratio and colority removal ratio under different reaction times.

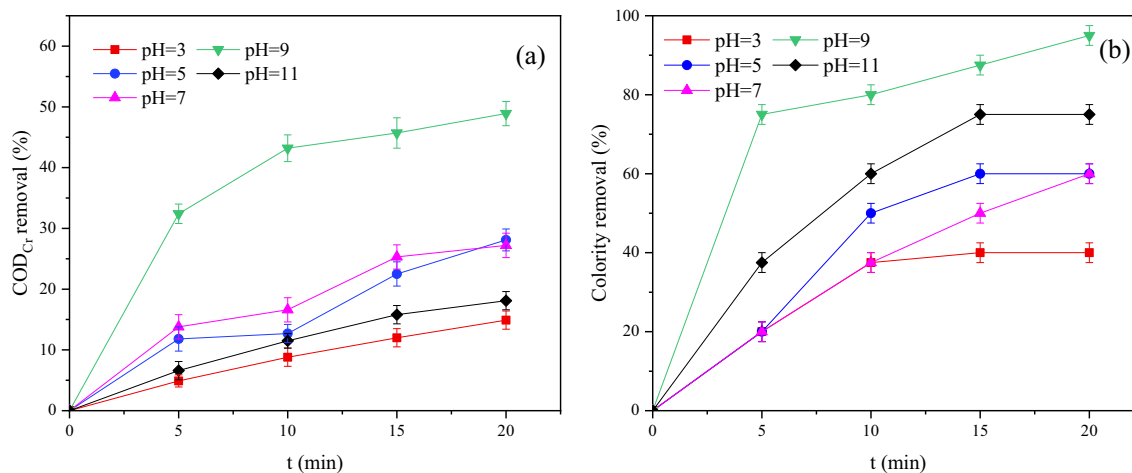
rapidly in a short period of time. Excessive HO<sup>•</sup> results in a quenching reaction that decreases the total amount of HO<sup>•</sup>, which causes the COD<sub>Cr</sub> removal ratio to decrease.

#### 3.4. Effects of catalyst dosage on catalytic ozonation using Mn-Fe-Ce/ $\gamma$ -Al<sub>2</sub>O<sub>3</sub>

Optimal conditions were obtained by selecting the above two single factors. Specifically, the reaction time was 20 min; thus, the dosage of ozone was 12.5 mg·L<sup>-1</sup>·min<sup>-1</sup>. In addition, the pH was 9. The catalyst dosages were selected as 0, 5, 10, 15,

and 25 g/L, respectively. The effects of different catalyst dosages on catalytic ozonation to remove COD<sub>Cr</sub> and colority were investigated, and the experimental results were shown in Fig. 7. When the dosage of the catalyst was 0–15 g/L, the removal ratio of COD<sub>Cr</sub> increased with the increasing of catalyst dosage, increases of 17.9%, 24.3% and 35.1% compared with ozone oxidation alone (0 g/L). The colority removal ratio achieved remarkable results when using the Mn-Fe-Ce/ $\gamma$ -Al<sub>2</sub>O<sub>3</sub> catalyst, and both values reached 95%. This finding indicated that the COD<sub>Cr</sub> removal ratio increased with as the catalyst increased under a certain dose. The increase in catalyst dosage provided a larger specific surface area and more active sites in the Mn-Fe-Ce/ $\gamma$ -Al<sub>2</sub>O<sub>3</sub> + O<sub>3</sub> system, which enhanced the catalyst's catalytic effect on ozone and produced more HO<sup>•</sup>. These effects also increased the COD<sub>Cr</sub> removal ratio (Shahamat et al., 2014).

Under a catalyst dosage of 25 g/L and a reaction time of 15 min, the COD<sub>Cr</sub> removal ratio of the Mn-Fe-Ce/ $\gamma$ -Al<sub>2</sub>O<sub>3</sub> + O<sub>3</sub> reaction system decreased to 19.8%. It is possible that an excessively large specific surface area and an excessive amount of active sites causing a quenching reaction to occur in the reaction system and significantly reduced HO<sup>•</sup> in the system. This result in the quantity and concentration of the HO<sup>•</sup> become very limited (Basturk and Karatas, 2015; Tabai et al., 2017). In this case, the reaction between HO<sup>•</sup> and refractory organics becomes slower. In the first 10 min, the refractory organics in the wastewater has not undergone major changes in the molecular structure under the oxidation of HO<sup>•</sup>, such as ring-opening reaction; thus, the organics cannot be oxidized by potassium dichromate. When the reaction proceeds for 15 min, the molecular structure of these refractory organics has undergone major changes under the sustained

**Fig. 6** COD removal ratio (a) and colority removal ratio (b) under different pH values.

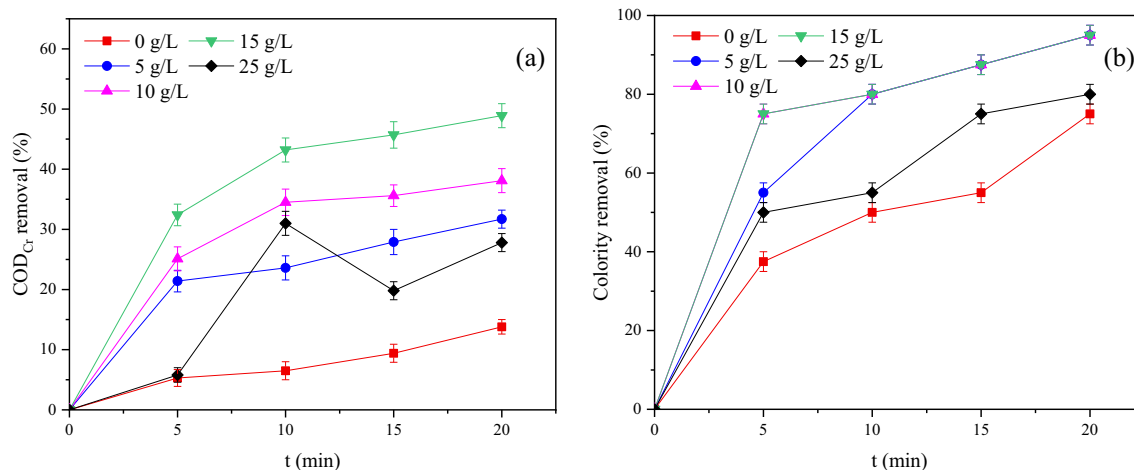


Fig. 7 COD<sub>Cr</sub> removal ratio (a) and colority removal ratio (b) under different catalyst dosages.

action of HO<sup>•</sup>. The intermediate products can also be oxidized by potassium dichromate. Therefore, the COD<sub>Cr</sub> removal ratio decreases. The above hypothesis must be confirmed by further investigation. In the setting gradient, the optimum value for the catalyst dosage is 15 g/L.

### 3.5. Improved biodegradability on catalytic ozonation using Mn-Fe-Ce/ $\gamma$ -Al<sub>2</sub>O<sub>3</sub>

To verify the effect of the Mn-Fe-Ce/ $\gamma$ -Al<sub>2</sub>O<sub>3</sub> + O<sub>3</sub> system on the biodegradability of dairy farming wastewater, the Biochemical Oxygen Demand (BOD<sub>5</sub>), COD<sub>Cr</sub>, Ammonia nitrogen content index (NH<sub>3</sub>-N), Total Phosphorus (TP) and colourity of pre-reaction wastewater and post-reaction wastewater were determined. The results are shown in Table 2.

As noted in the above table, after treatment with the Mn-Fe-Ce/ $\gamma$ -Al<sub>2</sub>O<sub>3</sub> + O<sub>3</sub> system, the change in NH<sub>3</sub>-N and TP concentration is small. In addition, COD<sub>Cr</sub> is greatly reduced, and BOD<sub>5</sub>/COD<sub>Cr</sub> is increased from 0.21 to 0.54. Biodegradability was significantly improved. These findings indicate that the HO<sup>•</sup> produced in the Mn-Fe-Ce/ $\gamma$ -Al<sub>2</sub>O<sub>3</sub> + O<sub>3</sub> system has converted some of the refractory organics in dairy farming wastewater into biodegradable organics (Chen et al., 2015).

### 3.6. Stability of catalyst

The stability of the catalyst was studied in 10 consecutive cycles under the following optimal conditions: ozone dosage was 12.5 mg·L<sup>-1</sup>·min<sup>-1</sup>, catalyst dosage was 15 g/L, pH was 9, and the reaction time was 20 min. The catalyst was reused to determine the COD<sub>Cr</sub> removal ratio of the dairy farming

wastewater and the leaching of Mn<sup>2+</sup>, Fe<sup>3+</sup>, Ce<sup>3+</sup>/Ce<sup>4+</sup> and Al<sup>3+</sup>.

As shown in Fig. 8, the COD<sub>Cr</sub> removal ratio was not changed as the number of catalysts used increased. Under a 20-minute reaction time, COD<sub>Cr</sub> removal ratio was 48.0% for the 10th recycled catalyst, and this value was only 0.9% lower than the initial COD<sub>Cr</sub> removal ratio of the catalyst. The COD<sub>Cr</sub> removal ratio curve clearly showed that the activity of the catalyst was significantly maintained in 10 cycles,

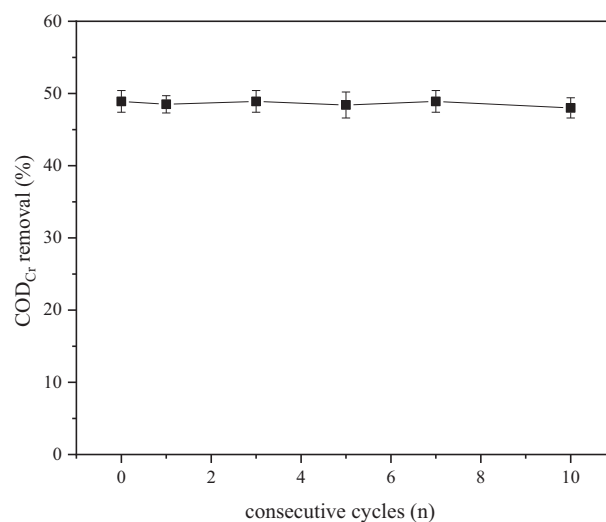


Fig. 8 COD<sub>Cr</sub> removal ratio using Mn-Fe-Ce/ $\gamma$ -Al<sub>2</sub>O<sub>3</sub> catalyst in 10 consecutive cycles.

Table 2 Effect of heterogeneous catalytic oxidation of microbubble ozone on biodegradability of dairy farming wastewater.

Water quality index	COD <sub>Cr</sub> (mg/L)	BOD <sub>5</sub> (mg/L)	BOD <sub>5</sub> /COD <sub>Cr</sub>	NH <sub>3</sub> -N (mg/L)	TP (mg/L)	Colourity (multiple)
Before treatment	460	98.4	0.21	59.09	7.52	160
After treatment	235	126.9	0.54	56.30	7.25	8

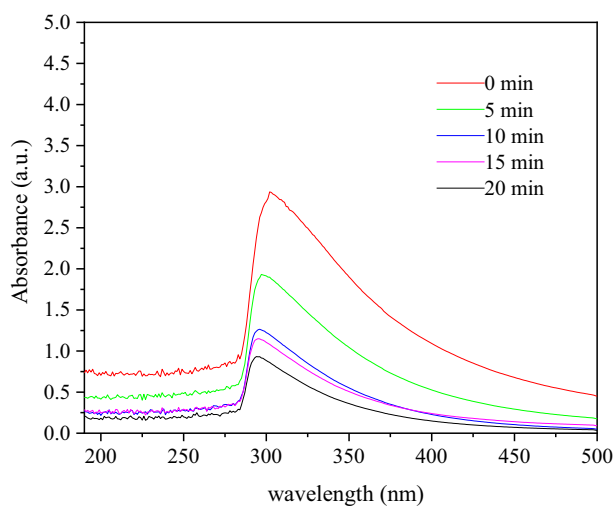
**Table 3** Elemental contents of the first, fifth, and tenth reused Mn-Fe-Ce/ $\gamma$ -Al<sub>2</sub>O<sub>3</sub> catalyst.

Consecutive cycles (n)	Mn (%)	Fe (%)	Ce (%)	Al (%)
0	11.7	17.6	10.2	56.5
1	11.6	17.3	10.0	56.5
5	11.5	17.0	10.0	56.4
10	11.0	16.9	9.5	56.3

**Table 4** Catalytic ozonation results of different wastewater onto different catalysts from literature reports.

Catalysts	Type of wastewater	Reaction condition	Catalytic performance				Ref.
			COD <sub>Cr</sub> removal ratio (%)	TOC removal ratio (%)	Colourity removal ratio (%)	BOD <sub>5</sub> /COD <sub>Cr</sub>	
$\beta$ -FeOOH/Al <sub>2</sub> O <sub>3</sub>	2,4-D (10 mg/L)	t = 40 min, 2 mg/L gaseous ozone concentration, pH = 6, 0.25 g/L catalyst	–	95	–	–	Nie et al.
Mn/ $\gamma$ -Al <sub>2</sub> O <sub>3</sub>	Phenol wastewater (100 mg/L)	t = 90 min, 8 mg/min gaseous ozone concentration, pH = 6.5, 1 g/L catalyst	–	82.7	–	–	Wang et al.
Mn-Cu-O/Al <sub>2</sub> O <sub>3</sub>	Refinery wastewater	t = 25 min, 50 mg/L gaseous ozone concentration, pH = 6.8, 3 g/L catalyst, T = 17	90	–	–	–	Deng et al.
Cu-Ce/Al <sub>2</sub> O <sub>3</sub>	Pulp and paper mill wastewaters	t = 60 min, 0.3 g/h gaseous ozone concentration, pH = 7.9, 5 g/L catalyst	–	61.5	95.3	0.17–0.37	He et al.
Mn-Fe-Cu/Al <sub>2</sub> O <sub>3</sub>	Petroleum refinery wastewater	t = 60 min, 2.19 g/h gaseous ozone concentration, pH = 8.2, 20 g catalyst, 0.4-MPa reaction pressure	69.4	–	–	0.098–0.330	Chen et al.
ZSM-5 zeolites	NBD-Cl (20 ppm)	t = 30 min, 0.6 mg/min gaseous ozone concentration, pH = 13, 2 g catalyst	60	–	–	–	Ikhlaiq et al.
Cobalt and manganese co-doped $\gamma$ -Fe <sub>2</sub> O <sub>3</sub> (FCM)	2,4-D (20 mg/L)	t = 40 min, 30 mg/L gaseous ozone concentration, pH = 6, 1 g/L catalyst	–	95	–	–	Aihua et al.
Mn-Fe-Ce/ $\gamma$ -Al <sub>2</sub> O <sub>3</sub>	Dairy farming wastewater	t = 20 min, 12.5 mg·L <sup>-1</sup> ·min <sup>-1</sup> gaseous ozone concentration, pH = 9, 15 g/L catalyst	48.9	–	95	0.21–0.54	Present study

indicating that the catalyst has a long usage life in the Mn-Fe-Ce/ $\gamma$ -Al<sub>2</sub>O<sub>3</sub> + O<sub>3</sub> system. In addition, Mn<sup>2+</sup>, Fe<sup>3+</sup>, Ce<sup>3+</sup>/Ce<sup>4+</sup> and Al<sup>3+</sup> in the reaction system undergo a certain degree of leaching during the reaction. The elemental contents of the first, fifth, and tenth reused Mn-Fe-Ce/ $\gamma$ -Al<sub>2</sub>O<sub>3</sub> catalysts are as shown in Table 3. The leaching amount of Mn<sup>2+</sup>, Fe<sup>3+</sup>, and Ce<sup>3+</sup>/Ce<sup>4+</sup> in the catalyst increases as the number of times the catalyst was used increases, while Al<sup>3+</sup> does not exhibit substantial leaching. The possible reason is that the purchased  $\gamma$ -Al<sub>2</sub>O<sub>3</sub> carrier is a small ball prepared by a special process after long high-temperature calcination, and Al<sub>2</sub>O<sub>3</sub> is stable and does not easily undergo leaching. Secondly, the active component is loaded on  $\gamma$ -Al<sub>2</sub>O<sub>3</sub>. The surface of the carrier is equivalent to the Al element surrounded by the active component, and the Mn<sup>2+</sup>, Fe<sup>3+</sup>, and Ce<sup>3+</sup>/Ce<sup>4+</sup> supported on the surface gradually leach over time during the reaction. Thus, the Mn-Fe-Ce/ $\gamma$ -Al<sub>2</sub>O<sub>3</sub> catalyst exhibits strong stability, ensures the catalytic effect of heterogeneous catalytic ozonation reaction, and provides the necessary foundation for its application in practical engineering. In addition, we have tabulated some examples about catalytic ozonation of wastewater

**Fig. 9** Ultraviolet spectrum of wastewater before and after microbubble ozone heterogeneous catalytic oxidation.

with different catalysts to discuss the differences between our research and existing research. The results are shown in Table 4.

### 3.7. Catalytic mechanism

The color-developing refractory organics in wastewater may be derived from the metabolites of feed, dairy cows or anaerobic microorganisms. Since the feed is mainly obtained locally, the water quality also exhibits certain regional and special characteristics. Ultraviolet spectroscopy was used to scan water samples with different reaction times. It can be seen from the results that the dairy farming wastewater has UV absorption at approximately 300 nm in Fig. 9. In addition, the absorption peak is obvious, and the absorbance is large. These findings indicate that most of the materials are complex organics containing a benzene ring structure and a phenolic

hydroxyl group. As the reaction progresses from 0 to 20 min, the absorption peak at 300 nm gradually becomes flat, indicating that the structure of the organic compound containing the benzene ring changes and transforms into the small molecule organics, which are gradually biodegraded.

HO $\cdot$  plays an important role in the heterogeneous catalytic oxidation of ozone. The reaction of most ozone involves heterogeneously catalytic oxidation that follows the HO $\cdot$  mediated oxidation mechanism (Chen et al., 2018; Deng et al., 2015; Ikhlaq et al., 2012). The use of Mn-Fe-Ce/ $\gamma$ -Al $_2$ O $_3$  as a catalyst improves the oxidation effect of the refractory organics in dairy farming wastewater. The main reason is that the metal oxide-loaded catalyst provides a large number of active sites on the surface of the carrier, promoting the generation of HO $\cdot$  (Salla et al., 2018; Yesiller et al., 2013; Ziylan-Yavař and Ince, 2018). When the pH value of the wastewater is close to the pH $_{pzc}$  value of the catalyst, the surface hydroxyl group in the neutral state is favorable for generating more HO $\cdot$  (Roshani et al., 2014; Wang Xu, 2012; Ye et al., 2016). As shown in Fig. 10, the effect of adding TBA on the COD $_{Cr}$  removal ratio shows that the hydroxyl group on the surface of Mn-Fe-Ce/ $\gamma$ -Al $_2$ O $_3$  promotes the formation of HO $\cdot$  (Sui et al., 2010; Vittenet et al., 2015; Wang et al., 2016). Compared with the sole ozone reaction, by loading the oxides of manganese, iron and ceria onto  $\gamma$ -Al $_2$ O $_3$ , the surface distribution of MnOOH, FeOOH and CeOOH on the catalyst is increased, which provides more active sites for the catalytic decomposition of ozone into HO $\cdot$  (Gonçaves et al., 2014; Laisheng et al., 2009; Restivo et al., 2016). Thus, the catalyst offers stronger oxidative capacity. In the Mn-Fe-Ce/ $\gamma$ -Al $_2$ O $_3$  + O $_3$  system, the surface hydroxyl group of Mn-Fe-Ce/ $\gamma$ -Al $_2$ O $_3$  initiates the decomposition of ozone and generates a large amount of HO $\cdot$ . The highly active HO $\cdot$  oxidized the organic pollutants in the water, causing the ring-opening reaction of the color-developing refractory organics to be converted into small molecule organics that are biodegraded (Bing et al., 2017; Wu et al., 2017). These small molecules of biodegradable organics can be further decomposed by the strong oxidant HO $\cdot$  and ozone in the aqueous phase to achieve mineralization.

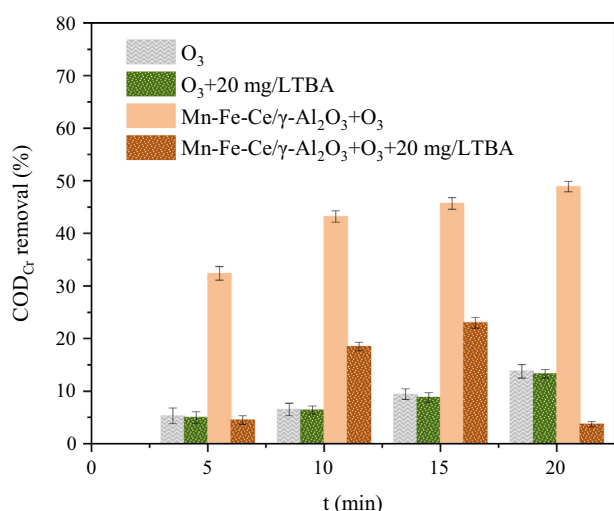


Fig. 10 Effect of TBA on degradation of dairy farming wastewater.

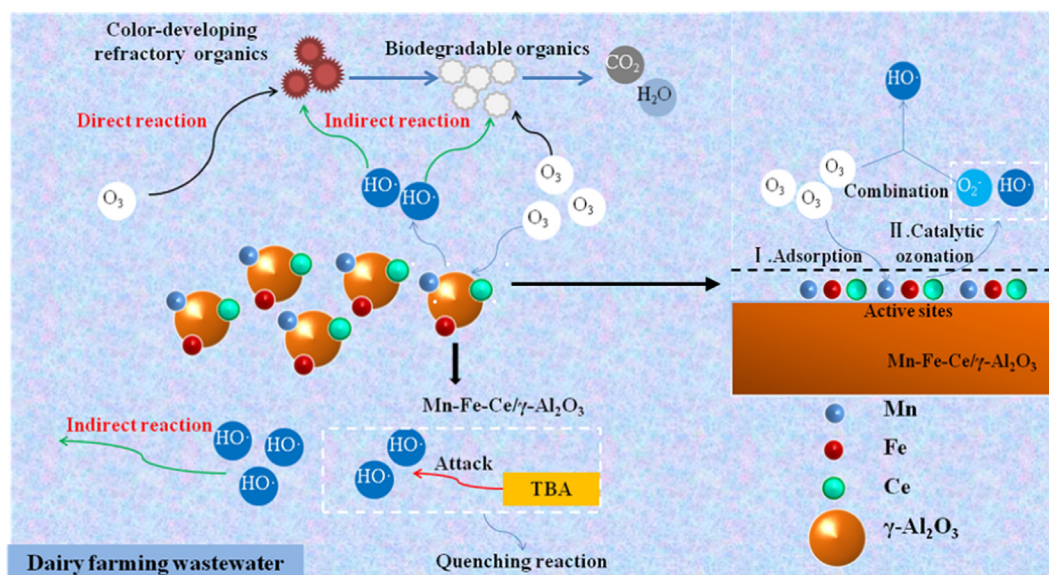


Fig. 11 Catalytic mechanisms in dairy farming wastewater using Mn-Fe-Ce/ $\gamma$ -Al $_2$ O $_3$ .

In addition, ozone in bulk can directly attack organic pollutants in wastewater to form intermediates instead of mineralization. Therefore, catalytic ozonation of dairy farming wastewater can achieve better treatment results using Mn-Fe-Ce/ $\gamma$ -Al<sub>2</sub>O<sub>3</sub> (see Fig. 11).

#### 4. Conclusions

The Mn-Fe-Ce/ $\gamma$ -Al<sub>2</sub>O<sub>3</sub> catalyst is obtained by impregnation and calcination of a precursor solution containing manganese, iron and cerium compounds. The SEM images showed that the active component was obviously attached to the surface of the  $\gamma$ -Al<sub>2</sub>O<sub>3</sub>. XRF analysis showed that the three elements Fe, Mn and Ce could be effectively supported on the surface of the  $\gamma$ -Al<sub>2</sub>O<sub>3</sub>. XRD analysis showed that the active component is formed on the surface of the catalyst, and the formation of a weak diffraction peak is related to the loading amount and the crystallization effect. Based on the catalytic activity and stability of Mn-Fe-Ce/ $\gamma$ -Al<sub>2</sub>O<sub>3</sub> catalyst, this study was first applied to the catalytic ozonation of dairy farming wastewater.

The catalytic performance of the Mn-Fe-Ce/ $\gamma$ -Al<sub>2</sub>O<sub>3</sub> catalyst for dairy farming wastewater was investigated using the simulated dynamic test. The optimum treatment conditions were as follows: reaction time was 20 min, ozone dosage was 12.5 mg·L<sup>-1</sup>·min<sup>-1</sup>, pH value was 9, and the catalyst dosage was 15 g/L. The COD<sub>Cr</sub> removal ratio of dairy farming wastewater can reach 48.9%, while colourity removal ratio can reach 95%. The BOD<sub>5</sub>/COD<sub>Cr</sub> increased from 0.21 to 0.54, which effectively improves the biodegradability and creates conditions for the continued use of biochemical methods for oxidized water.

The numerous hydroxyl groups on the surface of Mn-Fe-Ce/ $\gamma$ -Al<sub>2</sub>O<sub>3</sub> provide a rich active site for HO·, which causes the decomposition of ozone and generates a large amount of HO·. These effects significantly promote the conversion of the color-developing refractory organics into small molecule organics that can be biodegraded. The results showed that Mn-Fe-Ce/ $\gamma$ -Al<sub>2</sub>O<sub>3</sub> can be used as a catalyst for catalytic ozonation of dairy farming wastewater, which can provide better treatment efficiency and a new technical method for practical engineering applications.

#### Declaration of Competing Interest

The authors declare that they have no known competing financial interests or personal relationships that could have appeared to influence the work reported in this paper.

#### Acknowledgement

This work was supported by the Science and Technology Planning Project of Guangdong Province [grant numbers 2014A020209077].

#### References

- Aihua, L.V., Chun, H.U., Nie, Y., Jiuhui, Q.U., 2010. Catalytic ozonation of toxic pollutants over magnetic cobalt and manganese co-doped  $\gamma$ -Fe<sub>2</sub>O<sub>3</sub>. *Appl. Catal. B* 100, 62–67.
- Armenta, M.A., Valdez, R., Quintana, J.M., Silva-Rodrigo, R., Cota, L., Olivas, A., 2018. Highly selective CuO/ $\gamma$ -Al<sub>2</sub>O<sub>3</sub> catalyst promoted with hematite for efficient methanol dehydration to dimethyl ether. *Int. J. Hydrogen Energy* 43, 6551–6560.
- Basturk, E., Karatas, M., 2015. Decolorization of anthraquinone dye reactive blue 181 solution by UV/H<sub>2</sub>O<sub>2</sub> process. *J. Photochem. Photobiol., A* 299, 67–72.
- Bing, J., Hu, C., Zhang, L., 2017. Enhanced mineralization of pharmaceuticals by surface oxidation over mesoporous  $\gamma$ -Ti-Al<sub>2</sub>O<sub>3</sub> suspension with ozone. *Appl. Catal. B* 202, 118–126.
- Chen, C., Yan, X., Yoza, B.A., Zhou, T., Li, Y., Zhan, Y., Wang, Q., Li, Q.X., 2018. Efficiencies and mechanisms of ZSM5 zeolites loaded with cerium, iron, or manganese oxides for catalytic ozonation of nitrobenzene in water. *Sci. Total Environ.* 612, 1424–1432.
- Chen, C., Yoza, B.A., Wang, Y., Wang, P., Li, Q.X., Guo, S., Yan, G., 2015. Catalytic ozonation of petroleum refinery wastewater utilizing Mn-Fe-Cu/Al<sub>2</sub>O<sub>3</sub> catalyst. *Environ. Sci. Pollut. Res. Int.* 22, 5552–5562.
- Deng, F., Shan, Q., Cong, C., Xiao, D., Fang, M., 2015. Heterogeneous catalytic ozonation of refinery wastewater over alumina-supported Mn and Cu oxides catalyst. *Ozone Sci. Eng.* 37, 1–10.
- Faria, P.C.C., Órfão, J.J.M., Pereira, M.F.R., 2008. Activated carbon catalytic ozonation of oxamic and oxalic acids. *Appl. Catal. B* 79, 237–243.
- Feng, D., Zhou, J., Liu, W., Xue, Q., 2000. The thermal stability and lubricity of zinc thiomolybdenate at temperatures up to 500°C. *Wear* 246, 68–73.
- Feng, J., Zhang, X., Fu, J., Chen, H., 2018. Catalytic ozonation of oxalic acid over rod-like ceria coated on activated carbon. *Catal. Commun.* 110, 28–32.
- Ferreira, F.L.A., Jr, J.D.L., Amaral, L.A.D., 2003. Partial characterization of the polluting load of swine wastewater treated with an integrated biodigestion system. *Bioresour. Technol.* 90, 101–108.
- Gonçalves, A.G., Órfão, J.J.M., Pereira, M.F.R., 2014. Ozonation of erythromycin over carbon materials and ceria dispersed on carbon materials. *Chem. Eng. J.* 250, 366–376.
- He, S., Luan, P., Mo, L., Xu, J., Zeng, J., 2018. Mineralization of recalcitrant organic pollutants in pulp and paper mill wastewaters through ozonation catalyzed by Cu-Ce supported on Al<sub>2</sub>O<sub>3</sub>. *BioResources* 13, 3686–3703.
- Huang, N., Wang, W.-L., Xu, Z.-B., Lee, M.-Y., Wu, Q.-Y., Hu, H.-Y., 2019. A study of synergistic oxidation between ozone and chlorine on benzalkonium chloride degradation: reactive species and degradation pathway. *Chem. Eng. J.* 122856.
- Ikhlaq, A., Brown, D.R., Kasprzyk-Hordern, B., 2012. Mechanisms of catalytic ozonation on alumina and zeolites in water: Formation of hydroxyl radicals. *Appl. Catal. B* 123–124, 94–106.
- Ikhlaq, A., Brown, D.R., Kasprzyk-Hordern, B., 2013. Mechanisms of catalytic ozonation: an investigation into superoxide ion radical and hydrogen peroxide formation during catalytic ozonation on alumina and zeolites in water. *Appl. Catal. B* 129, 437–449.
- Juteau, P., Tremblay, D., Ould-Moulaye, C.B., Bisailon, J.G., Beaudet, R., 2004. Swine waste treatment by self-heating aerobic thermophilic bioreactors. *Water Res.* 38, 539–546.
- Khin, T., Annachhatre, A.P., 2004. Novel microbial nitrogen removal processes. *Biotechnol. Adv.* 22, 519–532.
- Kuang, C., Xu, Y., Lai, W., Xie, G., Pan, Z., Zheng, L., Talawar, M. P., Ling, J., Ye, S., Zhou, X., 2019. Novel electrodes for cathode electro-Fenton oxidation coupled with anodic oxidation system for advanced treatment of livestock wastewater. *Electrochim. Acta* 321, 134605.
- Laisheng, L., Weiyang, Y., Qiuyun, Z., Fengqiang, S., Ping, L., Xukai, L., 2009. Catalytic ozonation of dimethyl phthalate over cerium supported on activated carbon. *J. Hazard. Mater.* 170, 411–416.
- Li, X., Zhang, R., 2002. Aerobic treatment of dairy wastewater with sequencing batch reactor systems. *Bioprocess Biosyst. Eng.* 25, 103–109.
- Maleki, A., 2018. Green oxidation protocol: selective conversions of alcohols and alkenes to aldehydes, ketones and epoxides by using a new multiwall carbon nanotube-based hybrid nanocatalyst via ultrasound irradiation. *Ultrason. Sonochem.* 40, 460–464.
- Maleki, A., Hajizadeh, Z., Firouzi-Haji, R., 2018. Eco-friendly functionalization of magnetic halloysite nanotube with SO<sub>3</sub>H for synthesis of dihydropyrimidinones. *Micropor. Mesopor. Mater.* 259, 46–53.
- Maleki, A., Movahed, H., Ravaghi, P., Kari, T., 2016a. Facile in situ synthesis and characterization of a novel PANI/Fe<sub>3</sub>O<sub>4</sub>/Ag

- nanocomposite and investigation of catalytic applications. *RSC Adv.* 6, 98777–98787.
- Maleki, A., Rahimi, R., Maleki, S., 2016b. Efficient oxidation and epoxidation using a chromium(VI)-based magnetic nanocomposite. *Environ. Chem. Lett.* 14, 195–199.
- Najafian, A., Rabbani, M., Rahimi, R., Deilamkamar, M., Maleki, A., 2015. Synthesis and characterization of copper porphyrin into SBA-16 through “ship in a bottle” method: a catalyst for photo oxidation reaction under visible light. *Solid State Sci.* 46, 7–13.
- Ncanana, Z.S., Rajasekhar Pullabhotla, V.S.R., 2019. Oxidative degradation of m-cresol using ozone in the presence of pure  $\gamma$ - $\text{Al}_2\text{O}_3$ ,  $\text{SiO}_2$  and  $\text{V}_2\text{O}_5$  catalysts. *J. Environ. Chem. Eng.* 7, 103072.
- Nie, Y., Hu, C., Li, N., Yang, L., Qu, J., 2014. Inhibition of bromate formation by surface reduction in catalytic ozonation of organic pollutants over  $\beta$ - $\text{FeOOH}/\text{Al}_2\text{O}_3$ . *Appl. Catal. B* 147, 287–292.
- Nie, Y., Li, N., Hu, C., 2015. Enhanced inhibition of bromate formation in catalytic ozonation of organic pollutants over  $\text{Fe}-\text{Al LDH}/\text{Al}_2\text{O}_3$ . *Sep. Purif. Technol.* 151, 256–261.
- Restivo, J., Garcia-Bordejé, E., Órfão, J.J.M., Pereira, M.F.R., 2016. Carbon nanofibers doped with nitrogen for the continuous catalytic ozonation of organic pollutants. *Chem. Eng. J.* 293, 102–111.
- Rodríguez, E.M., Fernández, G., Alvarez, P.M., Beltrán, F.J., 2012.  $\text{TiO}_2$  and  $\text{Fe(III)}$  photocatalytic ozonation processes of a mixture of emergent contaminants of water. *Water Research.* 46, 152–166.
- Roshani, B., McMaster, I., Rezaei, E., Soltan, J., 2014. Catalytic ozonation of benzotriazole over alumina supported transition metal oxide catalysts in water. *Sep. Purif. Technol.* 135, 158–164.
- Salla, J.S., Padoin, N., Amorim, S.M., Li Puma, G., Moreira, R.F.P. M., 2018. Humic acids adsorption and decomposition on  $\text{Mn}_2\text{O}_3$  and  $\alpha$ - $\text{Al}_2\text{O}_3$  nanoparticles in aqueous suspensions in the presence of ozone. *J. Environ. Chem. Eng.* <https://doi.org/10.1016/j.jece.2018.11.025>.
- Santos, F., Almeida, C.M.R., Ribeiro, I., Mucha, A.P., 2019. Potential of constructed wetland for the removal of antibiotics and antibiotic resistant bacteria from livestock wastewater. *Ecol. Eng.* 129, 45–53.
- Sehested, K., Holcman, J., Bjergbakke, E., Hart, E.J., 1984. Formation of ozone in the reaction of  $\text{OH}$  with  $\text{O}_3$  and the decay of ozonide ion radical at pH 10–13. *J. Phys. Chem.* 88, 269–273.
- Shahamat, Y.D., Farzadkia, M., Nasser, S., Mahvi, A.H., Gholami, M., Esrafil, A., 2014. Magnetic heterogeneous catalytic ozonation: a new removal method for phenol in industrial wastewater. *J. Environ. Health Sci. Eng.* 12, 50.
- Sui, M., Li, S., Lu, K., Feng, T., 2010.  $\text{FeOOH}$  catalytic ozonation of oxalic acid and the effect of phosphate binding on its catalytic activity. *Appl. Catal. B* 96, 94–100.
- Sun, W., Sun, Y., Shah, K.J., Chiang, P.-C., Zheng, H., 2019. Electrocatalytic oxidation of tetracycline by  $\text{Bi-Sn-Sb}/\gamma\text{-Al}_2\text{O}_3$  three-dimensional particle electrode. *J. Hazard. Mater.* 370, 24–32.
- Tabaï, A., Bechiri, O., Abbessi, M., 2017. Degradation of organic dye using a new homogeneous Fenton-like system based on hydrogen peroxide and a recyclable Dawson-type heteropolyanion. *Int. J. Ind. Chem.* 8, 83–89.
- Vittenet, J., Aboussaoud, W., Mendret, J., Pic, J.-S., Debellefontaine, H., Lesage, N., Faucher, K., Manero, M.-H., Thibault-Starzyk, F., Leclerc, H., Galarneau, A., Brosillon, S., 2015. Catalytic ozonation with  $\gamma\text{-Al}_2\text{O}_3$  to enhance the degradation of refractory organics in water. *Appl. Catal. A* 504, 519–532.
- Wang, H., Mustafa, M., Yu, G., Östman, M., Cheng, Y., Wang, Y., Tysklind, M., 2019. Oxidation of emerging biocides and antibiotics in wastewater by ozonation and the electro-peroxone process. *Chemosphere* 235, 575–585.
- Wang, J.L., Xu, L.J., 2012. Advanced oxidation processes for wastewater treatment: formation of hydroxyl radical and application. *Crit. Rev. Environ. Sci. Technol.* 42, 251–325.
- Wang, Y., Yang, W., Yin, X., Liu, Y., 2016. The role of Mn-doping for catalytic ozonation of phenol using  $\text{Mn}/\gamma\text{-Al}_2\text{O}_3$  nanocatalyst: performance and mechanism. *J. Environ. Chem. Eng.* 4, 3415–3425.
- Wu, J., Su, T., Jiang, Y., Xie, X., Qin, Z., Ji, H., 2017. In situ DRIFTS study of  $\text{O}_3$  adsorption on  $\text{CaO}$ ,  $\gamma\text{-Al}_2\text{O}_3$ ,  $\text{CuO}$ ,  $\alpha\text{-Fe}_2\text{O}_3$  and  $\text{ZnO}$  at room temperature for the catalytic ozonation of cinnamaldehyde. *Appl. Surf. Sci.* 412, 290–305.
- Wu, J.J., Muruganandham, M., Chang, L.T., Lee, G.J., Batalova, V. N., Mokrousov, G.M., 2011. Catalytic ozonation of oxalic acid using  $\text{SrTiO}_3$  catalyst. *Ozone Sci. Eng.* 33, 74–79.
- Yang, P.Y., Chen, H.J., Kim, S.J., 2003. Integrating entrapped mixed microbial cell (EMMC) process for biological removal of carbon and nitrogen from dilute swine wastewater. *Bioresour. Technol.* 86, 245–252.
- Ye, W., Yang, W., Yin, X., Ying, L., 2016. The role of Mn-doping for catalytic ozonation of phenol using  $\text{Mn}/\gamma\text{-Al}_2\text{O}_3$  nanocatalyst: performance and mechanism. *J. Environ. Chem. Eng.* 4, 3415–3425.
- Yesiller, S.U., Eroğlu, A.E., Shahwan, T., 2013. Removal of aqueous rare earth elements (REEs) using nano-iron based materials. *J. Ind. Eng. Chem.* 19, 898–907.
- Ziylan-Yavaş, A., Ince, N.H., 2018. Catalytic ozonation of paracetamol using commercial and Pt-supported nanocomposites of  $\text{Al}_2\text{O}_3$ : the impact of ultrasound. *Ultrason. Sonochem.* 40, 175–182.